unlikely that the substituent could lead to so large a decrease in activation energy. While the discrepancy could well be due to error in the MNDO value, the good agreement for the inversion barrier suggests that our calculated classical barrier for the alternative mode of isomerization is also close to the truth. There is therefore a reasonable presumption that bond switching may take place by HAT because the observed rates are much greater than those corresponding to our calculated activation barrier. Tunnelling need not of course be considered in tub-to-tub inversion because this involves large changes in the positions of the atoms.

It tunnelling is indeed involved in bond switching, it must take place from the high energy planar isomer **22**; i.e., it must involve vibrationally activated tunnelling (VAT). As noted above, we have recently developed an approximate procedure for estimating the rates of such reactions. The calculated tunnelling (VAT) and classical rates are given in Table V. Even though our procedure is admittedly rather crude, there seems no doubt that the reaction takes place almost entirely by VAT because the differences between the VAT and classical rates are so large.

Acknowledgment. This work was supported by the Air Force Office of Scientific Research (Contract No. F49620-83-C-0024), the Robert A. Welch Foundation (Grant No. F-126), by the National Science Foundation (Grant No. CHE82-17948). We also thank Dr. Jimmy Stewart for helpful discussions during the course of this work.

Registry No. **3**, 34496-93-0; **6**, 28933-84-8; **9a**, 20829-57-6; **16**, 629-20-9.

Photodissociation of Acetylene at 193.3 nm

Alec M. Wodtke and Y. T. Lee*

Materials and Molecular Research Division, Lawrence Berkeley Laboratory, and Department of Chemistry, University of California, Berkeley, Berkeley, California 94720 *(Received: May 23, 1985)*

We have measured the translational energy release for processes $C_2H_2 \xrightarrow{193\ nm} C_2H + H$ (I) and $C_2H \xrightarrow{193\ nm} C_2 + H$ (II) using the molecular time-of-flight method. By measuring the maximum release of translational energy for process I it has been determined that the C–H bond energy in acetylene, $D_0(C_2H–H)$, is 132 ± 2 kcal/mol. Since the translational energy distribution peaks well away from zero, it is quite unlikely that internal conversion of the electronically excited C_2H_2 is an important channel for dissociation in channel I. Because of the relatively small amount of energy appearing as product rotation, it is possible to get information on the vibrational structure of C_2H radical from the translational energy distribution and it is found that the bending frequency in C_2H is 550 ± 100 cm^{-1}. Our experiment is consistent with earlier work which observed $C_2(^1\pi_u)$ in fluorescence.

Introduction

Acetylene is an important hydrocarbon in the area of combustion and has received a great deal of attention in the past. The ultraviolet spectrum in the 200-nm range was analyzed and found to be due to absorption to a trans-bent ^1A_u excited state.[1,2] Electron energy loss spectroscopy was used to place the approximate energy of two low-lying triplet states.[3] One aspect of this molecule which is still quite uncertain, however, is the C–H bond energy, $D_0(C_2H–H)$. The lowest dissociative ionization threshold, producing $C_2H^+ + H + e^-$, was measured to be 17.365 eV by Dibeler, Walker, and McCulloh[4] (DWM) and more recently in a molecular beam by Ono and Ng[5] (ON) to be 16.79 eV. Combining the ionization potential (IP) of C_2H radical[6,7] with these thresholds, $D_0(C_2H–H)$ can be derived. In an analogous way the electron affinity of C_2H[8] was combined in a thermochemical cycle with the acidity of C_2H_2[9] and the IP of H to give $D_0(C_2H–H)$. But due to the systematic deviations between experiments, the uncertainty in the determination of $D_0(C_2H–H)$ has not been smaller than 0.5 eV. Recently, ab initio calculations have given a bond energy of 127 kcal/mol with an estimated error of 2 kcal/mol.[10]

The advent and commercialization of excimer lasers (specifically ArF lasers at 193.3 nm) has allowed considerable advance in the study of the photochemistry of the ^1A_u absorption system. Irion and Kompa[11] have used an unfocused ArF laser to dissociate acetylene in a gas cell, analyzing the collisionally quenched, stable products with time-of-flight mass spectrometry. They concluded that C–H bond rupture is the primary, unimolecular dissociation pathway.

$$C_2H_2 \xrightarrow{193\ nm} C_2H + H \qquad (I)$$

McDonald, Baranovski, and Donnelly[12] and more recently Okabe, Cody, and Allen[13] have used a focused ArF laser (3×10^{26} photons/(cm^2 s)) to photolyze acetylene. They observed two- and three-photon absorption processes to form C_2 and CH in excited electronic states that were observed by dispersed fluorescence spectroscopy. Again, using a strongly forcused ArF laser, emission from electronically excited C atom was observed by Miziolek et al.[14]

In order to better understand the dynamics of the primary photodissociation processes involved and in an effort to nail down $D_0(C_2H–H)$ in acetylene, we have recently performed molecular beam experiments designed to measure the translational energy release of fragments from the photolysis of acetylene at 193.3 nm under collision free conditions.

Experimental Section

The experiments were performed on a new molecular beam apparatus designed specifically for crossed laser, molecular beam photodissociation studies. Some of the features of this machine

(1) Ingold, C. K.; King, G. W. *J. Chem. Soc.* **1953**, 2702.
(2) Innes, K. Keith *J. Chem. Phys.* **1954**, *22*, 863.
(3) Trajmar, S.; Rice, J. K.; Wei, P. S. P.; Kuppermann, A. *Chem. Phys. Lett.* **1968**, *1*, 703.
(4) Dibeler, Vernon H.; Walker, James A.; McCulloh, K. E. *J. Chem. Phys.* **1973**, *59*, 2264.
(5) Ono, Y.; Ng, C. Y. *J. Chem. Phys.* **1981**, *74*, 6985.
(6) Okabe, H.; Dibeler, V. H. *J. Chem. Phys.* **1973**, *59*, 2430.
(7) Berkowitz, J. "Photoabsorption, Photoionization, and Photoelectron Spectroscopy"; Academic Press: New York, 1979; pp 285–290.
(8) Janousek, B. K.; Brauman, J. I.; Simons, J. *J. Chem. Phys.* **1979**, *71*, 2057.
(9) Mackay, G. I.; Bohme, D. K. *Int. J. Mass Spectrom. Ion Phys.* **1978**, *26*, 327.
(10) Melius, Carl D.O.E. Proceedings of the Combustion Research Contractor's Metting, Sponsored by the Office of Basic Energy Sciences, U.S. Department of Energy, 1984; p 39.
(11) Irion, M. P.; Kompa, K. L. *Appl. Phys.* **1982**, *B27*, 183.
(12) McDonald, J. R.; Baranovski, A. P.; Donnelly, V. M. *Chem. Phys.* **1978**, *33*, 161.
(13) Okabe, H.; Cody, R. J.; Allen Jr., J. E. *Chem. Phys.* **1985**, *93*, 67.
(14) Private communication.

0022-3654/85/2089-4744$01.50/0

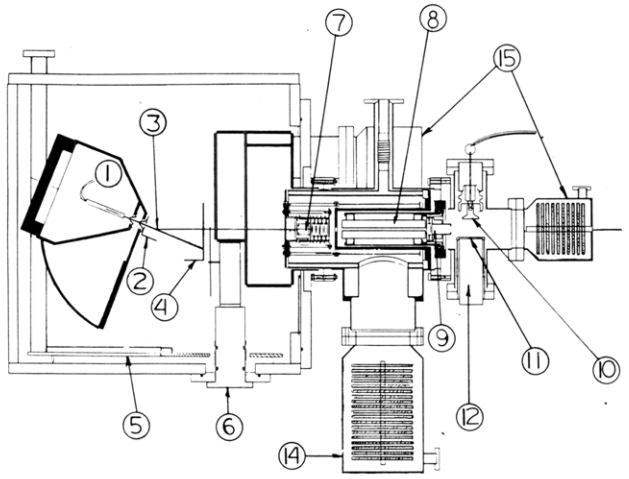

Figure 1. The new molecular beam photodissociation machine. (1) Gas feed line to nozzle. (2) Liquid helium cooled collimation slit. (3) Interaction zone. (4) Liquid nitrogen cooled beam catcher. (5) Liquid nitrogen cooled copper panels. (6) Removable time-of-flight wheel, for measuring primary beam velocity distribution. (7) Brink-type ionizer. (8) Quadrupole mass filter. (9) Exit ion optics. (10) Ion target. (11) Scintillator. (12) Photomultiplier tube. (14) Magnetically suspended turbomolecular pump. (15) Grease sealed turbomolecular pumps.

are shown in Figure 1. The instrument consists of three parts: a rotating molecular beam source, a fixed, ultrahigh vacuum, mass spectrometric detector , and a "main" interaction chamber.

A continuous molecular beam was formed by passing 250 torr of a 15% mixture of acetylene in neon through a dry ice ethanol trap to remove acetone and expanding it through a 0.125-mm nozzle into the source region. The source region is pumped by two 6-in. diffusion pumps which do not move with the rotating source and maintain a pressure of 10^{-4} torr when the beam is on. The beam is skimmed and a region of differential pumping intervenes between the source region and the main chamber. The differential region is normally at 10^{-5} torr and is pumped by a 350 L/s turbomolecular pump which rotates with the source. A pulsed laser beam, which propogates along the rotation axis of the beam source, crosses the molecular beam creating a pulse of dissociation products.

A small angular fraction of this pulse of products will travel through two regions of differential pumping, spreading as it goes due to the velocity distribution of the nascent products. The pulse of dissociation products is then ionized in a liquid nitrogen cooled chamber (typically 10^{-10} torr) by a Brink-type, electron-impact ionizer. Ions produced are directed through a quadrupole mass filter than to a Daly-type ion counter, made up of an ion target, a scintillator, and a photomultiplier tube. The transient pulse or time-of-flight (TOF) spectrum is recorded on a 255-channel scaler operating as a pulse counter with a minimum channel width of 1 μs which is triggered by the laser pulse. For high TOF resolution using a 1-μs channel width, a digital delay was introduced on the trigger of the multichannel scaler so that the transient pulse would be recorded in as many of the 255 channels as possible. The data acquisition is overseen and directed by a macro program running on a DEC LSI-11 lab computer. Typically, data produced by one million laser pulses are collected at a repetition rate of 150 Hz for each TOF spectrum.

The holes in the detector walls between 3 and 7 in Figure 1 are precision machined and define the "viewing window" of the detector. These are placed so that the detector "sees" all parts of the 3 mm × 3 mm × 1 mm interaction volume (at 3) for all angles to which the beam source can rotate. One might think that the background in the detector that is created by the operation of the molecular beam could be calculated from the conductance of the defining slits and the pumping speeds of the pumps on each region of differential pumping according to the following equation.

$$P_{\text{detector}} = P_{\text{main chamber}} \frac{C_1}{S_1} \frac{C_2}{S_2} \frac{C_3}{S_3}$$

TABLE I

expansion conditions	$\Delta V/V$	most probable velocity, cm/s	ΔE_T^{LAB}, kcal/mol
seeded, 300 K	12	7.9×10^4	1
seeded, 530 K	12	10.8×10^4	1
neat, 300 K	25	8.4×10^4	2

where P_{detector} = partial pressure in the detector, $P_{\text{main chamber}}$ = partial pressure in the main chamber, C_i = conductance of each differential pumping aperture, and S_i = pumping speed of each pump on each differential pumping region.

But for those molecules that travel straight through all of the differential pumping apertures, the above equation will not apply. This so-called "direct-through background" cannot be decreased by any number of differential pumping regions. When this is the limiting source of background in the detector, the above equation will always calculate a background level much lower than that which is experimentally observed. Since the pressure in the main chamber is 2×10^{-7} torr, the mean free path is much larger than the dimensions of the chamber itself. For this reason "direct through background" cannot come from collisions with other molecules within the viewing window of the detector. It can only be formed by first bouncing off of surfaces that are within the viewing window of the detector. Consequently a closed cycle refrigerator was used to cool a copper collimation slit to 30 K at 2 in Figure 1. This lowers the background, originating from the main chamber, by a factor of 10. In addition to this, liquid nitrogen is supplied to the main chamber and cools large copper panels which serve as cryopumps. Undissociated acetylene strikes one of these panels. This is an effective beam catcher for condensible gases.

Data analysis consists of finding the center-of-mass frame translational energy distribution function, $P(E_T)$, from the observed laboratory frame time-of-flight spectra. For the analysis of primary dissociation processes we use the "forward convolution" method. This means that we guess at a trial $P(E_T)$ and calculate what our data should look like, taking into consideration several instrumental averaging factors including beam velocity and angular dispersion, ionizer length, detector angular resolution, and multichannel scaler channel width. We then alter the $P(E_T)$ until the calculated TOF fits the data. For secondary dissociation (i.e., in the case where primary photolysis products are themselves photolyzed) we use a similar program which performs much more averaging. In a sense looking at secondary dissociation is like looking at a primary process with a very poorly defined molecular beam. In this forward convolution program, the entire primary dissociation flux map in the three-dimensional laboratory frame is calculated. This flux map is converted to number density and used to characterize the angular and velocity distributions of the "molecular beam" to which the primary process gives rise.

Experiments were done at two nozzle temperatures to observe the influence of unrelaxed bending vibrations in acetylene and also a neat beam of acetylene was used for low laser power experiments. Table I gives the beam characteristics.

The laser was a Lambda-Physik EMG 103 MSC excimer laser and was run with ArF. Typically, 100 mJ/pulse at 150 Hz were obtained and focused to a 1 mm × 3 mm rectangular spot.

Results and Analysis

Laser photolysis gives signal at mass-to-charge ratios (m/e) of 25, 24, 13, and 12 amu. From the comparison of TOF spectra we know that the signal at m/e 13 and 12 comes from electron-impact-induced dissociative ionization of neutral products of masses 25 and 24. The TOF spectra at 20° for ion masses 25 and 24 are shown in Figure 2. The m/e 25 signal can only come from C_2H radical produced in the photolysis process. C_2H^+ ion formed in the ionizer can easily fragment to C_2^+ and gives rise to some of the signal at m/e 24. If C_2H were the only neutral product the m/e 25 and 24 spectra would be identical, apart from a very small difference in the flight time of the ions. The m/e 24 spectrum shows a substantial amount of signal arriving at significantly shorter arrival times (higher translational energies)

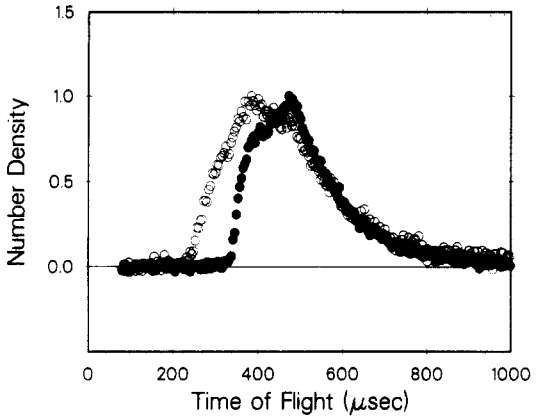

Figure 2. Mass 25 and 24 time-of-flight spectra. The open circles are m/e 24, the closed circles are m/e 25. Signal was observed at a source angle of 20°.

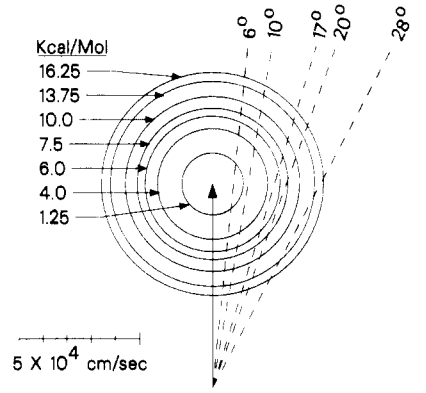

Figure 3. Newton diagram for seeded beam at 300 K. The angles shown are where data were taken. The circles represent the velocities of the C_2H radical produced in process I and the corresponding center-of-mass, relative, kinetic energies.

than the C_2H product. As will be shown in the next section from the laser power dependence of the dissociation signal, processes I and II which involve sequential photolysis of C_2H product during the laser pulse are responsible for the observed data.

$$C_2H_2 \xrightarrow{193\ nm} C_2H + H \qquad (I)$$

$$C_2H \xrightarrow{193\ nm} C_2 + H \qquad (II)$$

The determination of $D_0(C_2H-H)$ in acetylene relies on the principle of conservation of energy. When acetylene absorbs a photon at 193.3 nm it has 148 kcal/mol of energy at its disposal. We assume that the C_2H radical appearing with maximum translational energy corresponds to the ground-state fragment. The validity of this assumption will be discussed later. The difference between the photon energy and the maximum translational energy release is $D_0(C_2H-H)$. Although we can neglect any rotational energy of the parent acetylene which is well relaxed during the supersonic expansion, we cannot ignore unrelaxed vibrational energy in the two doubly degenerate bending modes which can contribute to the translational energy of the products. The frequencies of these two vibrations are 611 and 729 cm^{-1} which corresponds to about $3kT$ at room temperature. These will not be cooled efficiently in the supersonic expansion. In principle, one could remove these "hot bands" by cooling the nozzle, but in practice it is necessary to avoid cluster formation at low temperatures by heating the nozzle and identifying the contribution from the bending modes by observing a temperature-dependent increase in the fastest products.

A. Time-of-Flight Spectra of C_2H at 300 K Nozzle Temperature. Figure 3 shows the Newton diagram of the photolysis experiment for the 15% acetylene seeded in neon beam maintaining the nozzle temperature at 300 K. The purpose of a Newton diagram is to clarify the relationship between the lab frame of

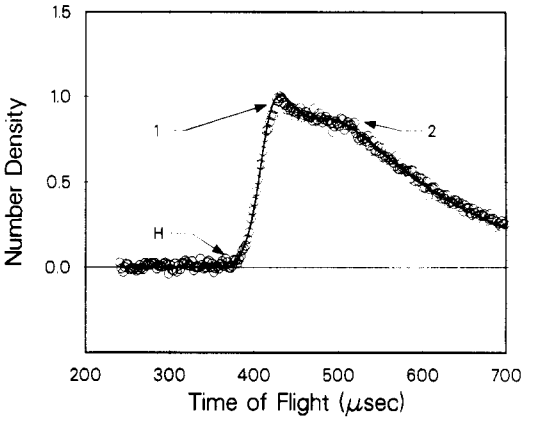

Figure 4. Time of flight spectrum of m/e 25 at a laboratory angle of 28° (the symbols refer to Figure 9).

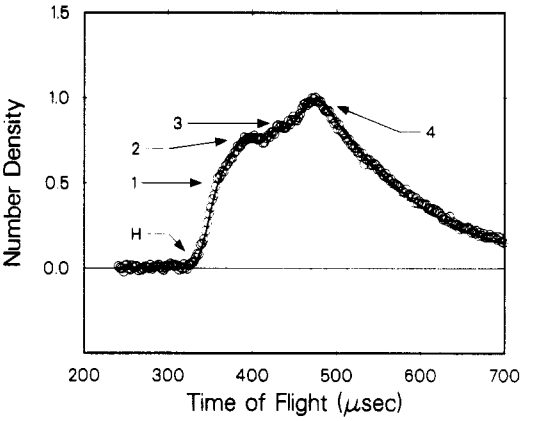

Figure 5. Same as Figure 4, but laboratory angle is 20°.

reference and the center-of-mass frame of reference. The bold arrow represents the molecular beam velocity in the lab frame. The center-of-mass of the system travels inertially along this vector. Vectorially adding the beam velocity vector to any center-of-mass frame vector yields the corresponding laboratory frame vector. The circles which are drawn centered on the tip of the beam vector indicate various recoil speeds in the center-of-mass frame of reference for the C_2H fragment, that is, all lab velocities observed on a given circle are from the same center-of-mass recoil speed of the dissociating fragment. Figure 3 indicates the relative translational energy release to which these C_2H fragment speeds correspond for process I. One can see that molecules with a large amount of internal excitation and hence low center-of-mass translational energies will not be scattered far from the beam. It is therefore necessary to look as close as 6° to the beam to see the most internally excited products. A more subtle experimental consideration comes from the fact that the resolution of the measurement of the laboratory velocity is limited by the ratio of the length of the ionizer to the total flight length, according to the following relationship.

$$\frac{\Delta V_{LAB}}{V_{LAB}} = \frac{\Delta t}{t} = \frac{\Delta L}{L} = \frac{1\ cm}{37\ cm} \cong 0.03 \qquad (1)$$

where ΔL = ionizer length (1 cm), L = flight length (37 cm), ΔV_{LAB} = lab velocity resolution element, V_{LAB} = lab velocity, Δt = arrival time resolution element, and t = arrival time. From this equation once can see that at high lab velocities a certain velocity difference will be spread out in time to a lesser extent than at low lab velocities. Also, at large laboratory angles, in addition to the fact that the lab velocity for a given Newton circle is smaller, the separation between a pair of Newton circles in laboratory velocity space is larger. Therefore, it is always better to look at large angles to get better resolution of the fast products.

Figures 4–9 show the data obtained at 28°, 20°, 17°, 10°, and 6° as well as the center-of-mass translational energy probability

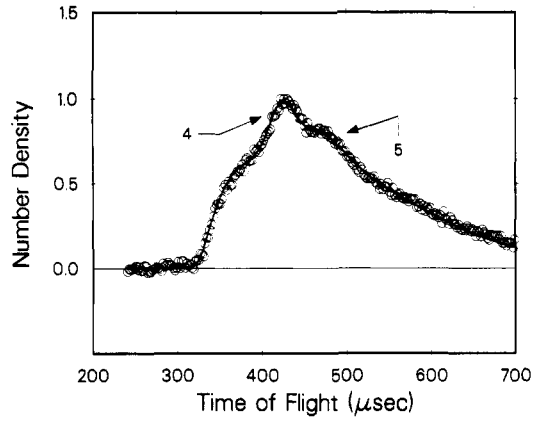

Figure 6. Same as Figure 4, but laboratory angle is 17°.

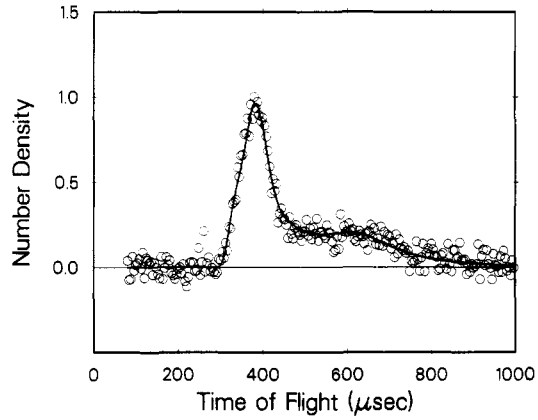

Figure 7. Same as Figure 4, but laboratory angle is 10°.

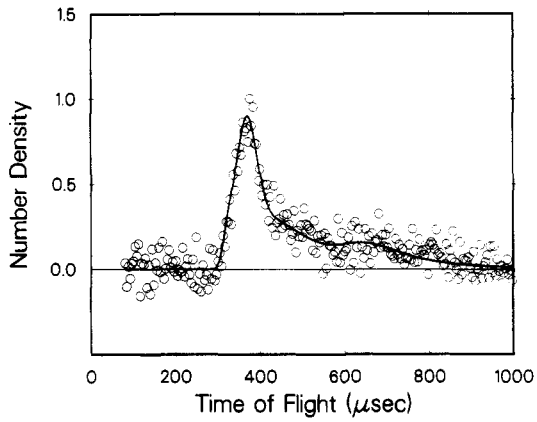

Figure 8. Same as Figure 4, but laboratory angle is 6°.

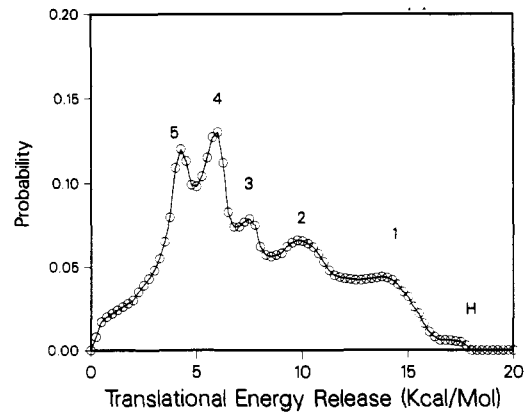

Figure 9. Translational energy probability distribution used to fit data in Figures 4–8.

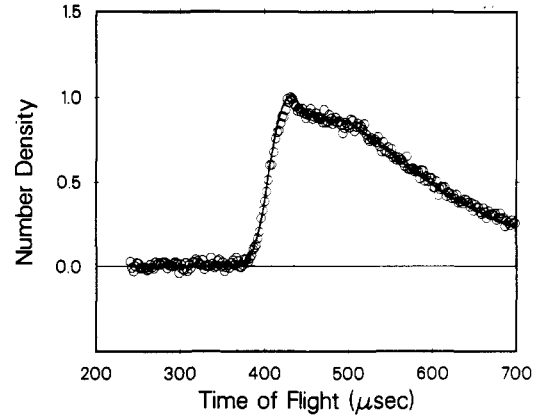

Figure 10. Time-of-flight spectrum at m/e 25 and a laboratory angle of 28°. The solid line is obtained by using the $P(E_T)$ in Figure 12.

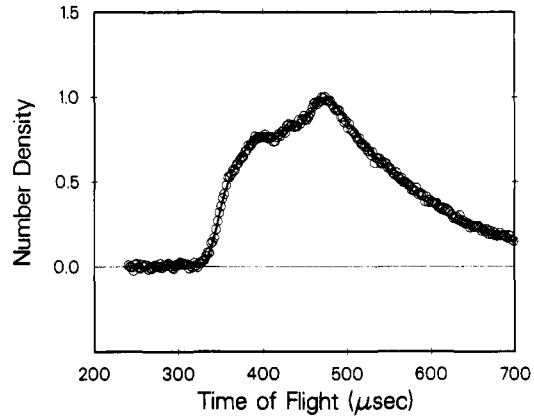

Figure 11. Same as Figure 10, but laboratory angle is 20°.

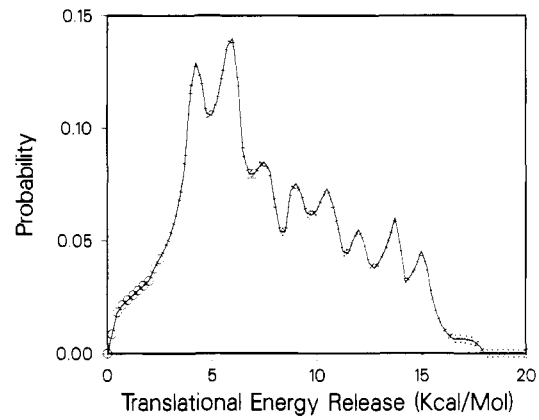

Figure 12. Translational energy probability distribution used to fit data in Figures 10 and 11.

distribution, $P(E_T)$ used to fit the data. In Figures 4–8, the circles are the data and the solid lines are the fit to the data. The structure that is being partially resolved is due to the internal state population distribution of the nacent C_2H radical. The peaks in the $P(E_T)$, Figure 9, have been labeled with arbitrary symbols and correspond to the like labeled bumps and shoulders in the TOF spectra. Experimentally, the peaks marked 1 and 2 are the least well determined. The $P(E_T)$ shown has the minimum structure necessary to fit the data. Figures 10, 11, , and 12 show a highly structured $P(E_T)$ and the fit it gives to the data. One can see that the data is not sensitive to these high-frequency oscillations for products which are formed with high translational energy.

B. Time-of-Flight Spectra of C_2H at 530 K Nozzle Temperature. In order to determine the effect of unrelaxed bending vibrations in C_2H_2 on the determination of the maximum release of translational energy, the nozzle was heated to 530 K, about tripling (in comparison to the 300 K experiment) the number of

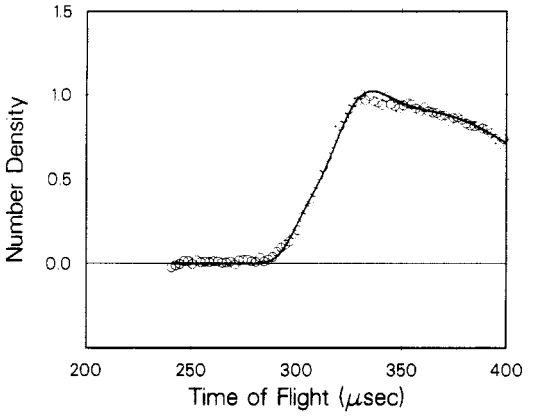

Figure 13. Time-of-flight spectrum of m/e 25 at a laboratory angle of 21° for a nozzle temperature of 530 K.

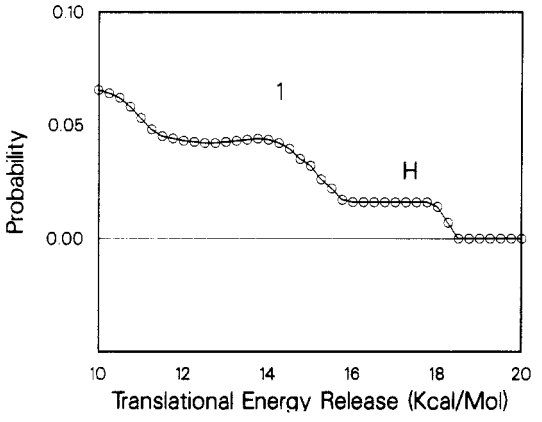

Figure 14. Translational energy probability distribution used to fit data in Figure 13.

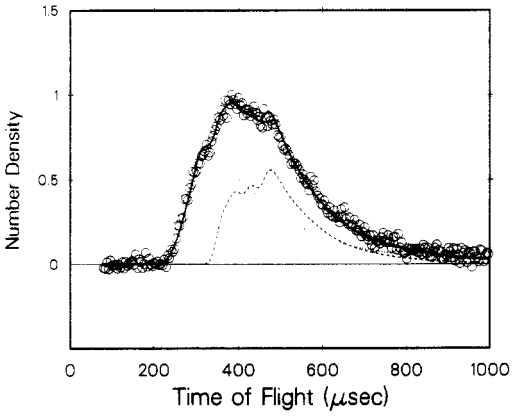

Figure 15. Time-of-flight spectrum of m/e 24 at a laboratory angle of 20°. The solid line is the total calculated TOF, the dashed line is the contribution from C_2H, and the dotted line is the contribution from C_2.

parent acetylene molecules not in the ground vibrational state. The TOF at 21° is shown in Figure 13 along with the best fit $P(E_T)$ in Figure 14. One can see that the fast peak labeled "H" (for hot bands) has increased in intensity with respect to the other peaks by about a factor of 3. We therefore conclude that the maximum release of translational energy occurs not at 18 kcal/mol but at slightly more than 16 kcal/mol, giving a $D_0(C_2H-H)$ of 132 kcal/mol.

C. Secondary Dissociation. Figures 15 and 16 show the m/e 24 (C_2^+) TOF and the best $P(E_T)$ which fits the data after removing the contribution from C_2H fragment. Although there is considerably less detail in the $P(E_T)$, the qualitative features are still apparent. The $P(E_T)$ appears to have two components. One is a sharp peak at about 10 kcal/mol and the other is a broad hump extending out to the maximum allowed translational energy. The

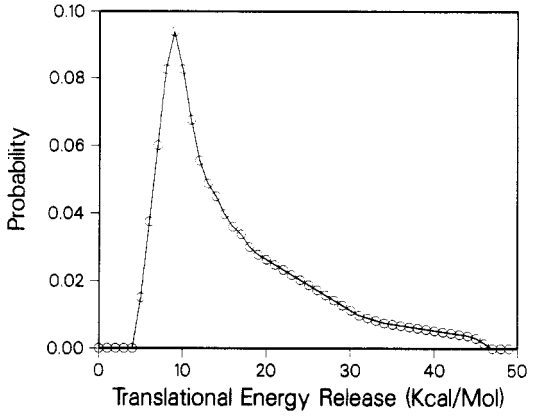

Figure 16. Translational energy distribution used to fit C_2 contribution to Figure 15.

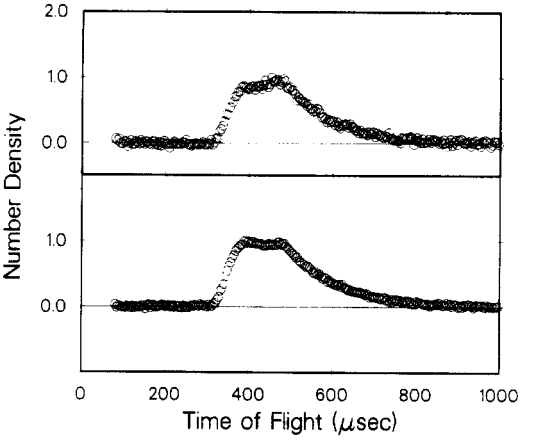

Figure 17. Time-of-flight spectra at different laser powers at m/e 25 and a laboratory angle of 20°. The upper trace is at 5 mJ/pulse and the lower trace is at 100 mJ/pulse.

maximum release of translational energy which includes the internal excitation of C_2 fragment indicates that C_2H has absorbed only one photon.

Discussion

A. Observed Collision Free Processes. The observation of laser induced m/e 25 signal at angles as large as 28°, and at lab velocities nearly twice that of the primary beam, is conclusive evidence that C_2H radical is being photochemically produced in the collision-free environment of a molecular beam. The amount of energy released as product translational motion is consistent with a single photon being absorbed. Although this is hardly a surprising finding, the presence of C_2H has always been inferred in past studies,[11-13] while this is the first direct observation of the nascent C_2H radical in the gas phase.

There are two conceivable explanations of our m/e 24 data: a sequential photodissociation described by processes I and II or a two-photon absorption creating a very highly excited C_2H_2 and subsequent decay as shown in process III. Consideration of the

$$C_2H_2 \xrightarrow{2 \times 193\ nm} H + C_2 + H \qquad \text{(III)}$$

$P(E_T)$ for the two-photon dissociation allows us to eliminate a simultaneous dissociation mechanism for process III. In a simultaneous, three-particle production process, conservation of linear momentum would require the two hydrogen atoms to be emitted in exactly the same direction in order to produce C_2 at as large a laboratory-frame velocity as we are observing. Even in a cis-bent excited state it is difficult to imagine a concerted dissociation mechanism that would do this. If the two-photon absorption of acetylene led to sequential loss of hydrogen atoms with time for the intermediate C_2H to rotate, it is possible that both hydrogen atoms could be emitted in the same direction. Similarly, the sequential mechanism involving processes I and II

would have no problem conforming to this constraint.

While there is no way to prove that process III is unimportant, there is compelling evidence for the existence of process II in the power dependent TOF spectrum at m/e 25 shown in Figure 17. These spectra were taken with a neat acetylene beam for maximum signal. It has close to the same velocity as the neon seeded beam but the velocity distribution is nearly twice as broad. The upper trace shows the TOF spectrum taken at low power, 5–10 mJ/pulse, while the lower trace shows the spectrum at close to 100 mJ/pulse. If process III were dominant we would expect only the magnitude and not the shape of the TOF to change with power. If process II dominates it is not at all unlikely that certain internal states of the C_2H radical would have a higher absorption cross section at 193.3 nm than others. This would give rise to a change in the shape of the m/e 25 TOF as a function of laser power, due to differential depletion of the C_2H radical, and that is exactly what has been observed in this experiment. Further evidence for the importance of process II is the calculation of Shih et al.[15] The results of their ab initio calculations on C_2H radical show that the two lowest doublet states above the $A^2\pi$ state are both in the vicinity of an ArF laser photon. The symmetries of these state are such that they would both be dipole allowed transitions. One of these states ($3^2A'$) correlates directly to $C_2(^1\pi_u)$ + H as observed in fluorescence[12,13] and in this work (see below).

We do not see any obvious evidence for the molecular elimination channel IV. The light H_2 products scatter in a much wider

$$C_2H_2 \xrightarrow{193\text{ nm}} C_2 + H_2 \qquad \text{(IV)}$$

laboratory angular and velocity range than do the C_2 fragments. In addition, the smaller ionization cross section and shorter residence time in the ionizer for H_2 make it harder to detect than heavier fragments such as C_2H and C_2. It is also very difficult to detect H_2 because of the very high m/e 2 background found in our mass spectrometer. We must, therefore, confine our search to looking for C_2. Because of the small release of translational energy that is possible (4 kcal/mol at most), we can look at m/e 24 data at 20° and be assured that there is no contribution from process IV. If we then use the $P(E_T)$'s derived from the 20° data to fit the data at m/e 24 and 10°, where we would be able to see process IV if it were present, we can get an upper limit to the importance of this channel by adding in the contribution from process IV little by little until the data are no longer fit. Sensitivity to the observation of this channel depends upon the amount of translatioal energy released in process IV. If less translational energy is released, channel IV is easier to see. In estimating a conservative upper limit to the importance of this channel we have assumed the worst case, that all of the available 4 kcal/mol appears as translation. This "masks" channel IV in the TOF so that it could appear very inconspicuously. Taking into consideration the relative ionization efficiencies of C_2 and C_2H to give C_2^+, this leads to an upper limit for process IV of 15% of process I. This is a very conservative estimate, since if the translational energy release is less (say 2 kcal/mol) then the branching ratio would be less than 2%. The quantum yield of the process for $C_2H_2 \rightarrow C_2 + H_2$ was estimated by Okabe[16] to be about 10% at 184.9 nm; however, the quantum yield is expected to be much smaller at 193 nm, since the photon energy is much closer to ΔH of the reaction forming $C_2 + H_2$.

It should be mentioned that we also did not observe CH product which is due to process V. Channel V was a minor channel

$$C_2H_2 \xrightarrow{2 \times 193\text{ nm}} 2CH \qquad \text{(V)}$$

observed optically in ref 10 and 11. McDonald et al. determined that (V) is less than 1% of the two-photon process that produces C_2. This would almost certainly be beyond our limit of detection. In summary, Table II lists the observed channels in this work as well as some channels that have been postulated, but not observed in this experiment.

TABLE II

channel	label	obsd
$C_2H_2(^1\Sigma_g^+) \xrightarrow{193\text{ nm}} C_2H(^2\pi, ^2\Sigma) + H$	I	yes
$C_2H \xrightarrow{193\text{ nm}} C_2(^1\Sigma_g^+, ^3\pi_u) + H$	II	yes
$C_2H \xrightarrow{193\text{ nm}} C_2(^1\pi_u) + H$	II	yes
$C_2H_2(^1\Sigma_g^+) \xrightarrow{2 \times 193\text{ nm}} C_2 + H_2$		no
$C_2H_2(^1\Sigma_g^+) \xrightarrow{193\text{ nm}} C_2 + H_2$	IV	<0.15 of I

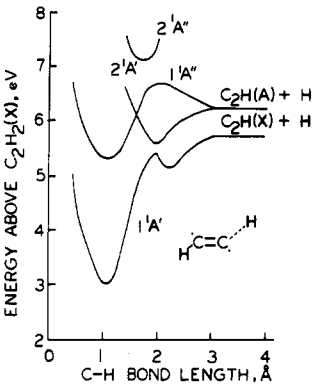

Figure 18. Schematic representation of the PES's for acetylene dissociation based on the calculations of Vasquez.

B. $P(E_T)$ for $C_2H_2 \xrightarrow{193\text{ nm}} C_2H + H$. Because of the conservation of total energy, in an experiment with infinite resolving power the $P(E_T)$ would appear as a series of discrete peaks, one corresponding to each internal quantum state of the C_2H radical, since only the $^2S_{1/2}$ state of H atom can be populated at these energies. Although it is not practical to resolve rotational quantum states of polyatomic molecules in velocity measurements, structure due to the vibrational state distribution can be observed in a favorable situation. In this experiment, we are able to see significant structure in the $P(E_T)$ due to the internal quantum state distribution of the C_2H. This is due primarily to the small amount of energy appearing as product rotation. Acetylene to rotationally cold in the beam so the rotational excitation of C_2H product will come only from repulsive bond rupture in which the orbital angular momentum of the departing fragments will be cancelled exactly by the rotational excitation of C_2H. But the creation of this pair of antiparallel angular momenta is constrained by the small mass of the departing hydrogen atom, the limited excess energy, and the impact parameter of the half-collision. One can see that information on the vibrational structure of C_2H radical is available through the $P(E_T)$.

Because the $A^2\pi$ state of C_2H is only 3692 cm^{-1} above the $X^2\Sigma$ state,[17] we must first decide which electronic states of C_2H are being formed in the photolysis at 193.3 nm. To understand this, one would like to see the electronic state correlation diagram for process I. The calculation of the potential energy surfaces (PES's) that are involved in the dissociation has not, as yet, been done. However, Vazquez has calculated the eight lowest surfaces for bent geometries of HCN,[18] which is isoelectronic with C_2H_2. Figure 1 of their paper serves as a guide to what the surfaces for acetylene would look like. Our Figure 18 is a schematic representation of the corresponding curves for excited C_2H_2 based on the calculations of Vazquez.

There are, undoubtedly, many differences between HCN and C_2H_2. For instance, the $1^1A''$ origin should be lower than the bond dissociation energy for acetylene. So, we expect that the avoided crossing between $1^1A''$ and $2^1A''$ will be lower in energy and occur at a longer C–H bond length than in HCN. Another difference occurs between CN and C_2H. In CN the $B^2\Sigma$ state is only 3.2 eV above the $X^2\Sigma$ state, while in C_2H the $B^2\Sigma$ is calculated to be 7.3 eV higher than $X^2\Sigma$.[13] For this reason, we do not expect that the surface that is analogous to the $3^1A'$ surface in Figure

(15) Shih, S. K.; Peyerimhoff, S. D. *J. Mol. Spectrosc.* **1979**, *74*, 124.
(16) Okabe, H. *J. Chem. Phys.* **1983**, *78*, 1312.
(17) Carrick, P. G.; Merer, A. J.; Curl Jr., R. F. *J. Chem. Phys.* **1983**, *78*, 3652.
(18) Vazquez, G. J. *Nuovo Cimento* **1981**, *63*, 446.

1 of ref 17 will influence the dynamics of acetylene at the energies found in our experiment.

Despite these differences, we do expect the qualitative features of Vazquez' Figure 1 to apply in the case of acetylene. In particular, the avoided crossing between the $1^1A''$ and the $2^1A''$ curves should be present. In our experiment we pump C_2H_2 to the $1^1A''$ curve of Figure 18. This state is diradical-like, with a C–C bond order of 2 and it is trans-bent.[1] It resembles ethylene with two diagonally opposed H's removed. The avoided crossing is the quantum mechanical representation of the rearrangement of the electronic configuration that is necessary in going from this diradical structure with a C–C double bond to the electronic structure of C_2H ($A^2\pi$) where the bond order is 2.5 and there is only one free radical electron.

The avoided crossing between X^1A' and $2^1A'$ shown in Figure 18 occurs only for significantly bent geometries. $X^2\Sigma$ C_2H has all π orbitals filled and a half-filled σ_{pz} orbital. For bent geometries the incoming H feels a new repulsion due to its interaction with the closed π orbitals. In contrast $A^2\pi$ C_2H has a filled σ_{pz} orbital and a half-filled π orbital (as well as a degenerate filled π orbital). For bent geometries the incoming H atom breaks the degeneracy of the π orbitals. There is a strong attraction to the half-filled π orbital, while there is a strong repulsion toward the filled π orbital. This avoided crossing has been invoked to explain the formation of $X^2\Sigma$ CN in the photodissociation of HCN.[18] It is likely that this avoided crossing occurs even more easily in C_2H since the separation of the X and A states is much smaller in C_2H than in CN.

Figure 18 has been constructed with the previous considerations taken into account and is meant as a qualitative picture of the dissociation process. Using Figure 18 as a guide we see that after acetylene is initially pumped to the $1^1A''$ its total energy, which is 6.4 eV, may well be less than the barrier height in the exit channel of this surface. Since the vibrational energy initially deposited in the molecule is mainly in the bending degree-of-freedom, even if the photon energy is slightly above the barrier height, the barrier will act as a bottleneck to $C_2H(A^2\pi)$ formation. We expect that the barrier will at least slow down the production of C_2H ($A^2\pi$) enough that vibronic coupling from $1^1A''$ to $2^1A'$ will become a competing dissociation pathway. Because of the repulsive nature of the $2^1A'$ surface and the consequent large H atom velocity, the curve hopping to the X^1A' surface will be very efficient. It is therefore not unreasonable that both electronic states of C_2H are being formed in our experiment and that they should be formed with a significant release of translational energy, as observed.

We do not believe that vibronic coupling to the X^1A' state is an important dissociation pathway. When formaldehyde was pumped 1 eV above its S_1 origin, it was found that vibronic coupling to S_0 and subsequent C–H bond rupture was the dominant process.[19] However, because dissociation on the S_0 PES involves a smooth and continuous rearrangement of the bonding electrons in formaldehyde to nonbonding, free-radical electrons in HCO and H, there is no barrier to dissociation. It is for this reason that simple bond rupture reactions that occur along the ground electronic surface so often lead to $P(E_T)$'s that peak near zero kinetic energy release. This was indeed observed in the formaldehyde experiment. Since this is in sharp contrast to acetylene, it is not likely that internal conversion to X^1A' is an important decay channel in our experiment.

The underlying broad structure between 0 and 6 kcal/mol is tentatively assigned to $C_2H(A^2\pi)$. Because of the poor quality of the data at small laboratory angles, corresponding to high internal energy fragments, it is presumptuous to estimate a branching ratio, but it does appear that most of the C_2H is being formed in the ground electronic state.

It is important next to consider the partitioning of energy into the vibrational degrees of freedom. If one assumes that our experiment resolves all the vibrational quantum states populated by the photolysis, then the widths of the peaks are due to solely to rotational excitation. One would be tempted to make the assignment of peaks 1, 2, 3, and 5 to the ν_3 bending vibration of C_2H with a frequency of about 1100 cm^{-1}. Peak 4 could then easily be assigned to $v = 1$ of the C–H stretch (ν_1) observed in marix at 3612 cm^{-1}.[20] However, $\nu_2 = 1100$ cm^{-1} is quite different than C_2H_2 bends of 600–700 cm^{-1}. In fact, there is no spectroscopic determination of the bending frequency in C_2H. Carrick et al.[17] estimate it from l-type doubling measurements to be between 390 and 475 cm^{-1} adding the caveat that vibronic coupling to the $A^2\pi$ state might increase the uncertainty of this estimate. Without further spectroscopic evidence and because peaks 1 and 2 are the least well determined features of the $P(E_T)$ (see Results and Analysis, section A), we would not recommend this assignment.

A more likely explanation of the $P(E_T)$ would label the most closely spaced peaks, which are also the most accurately determined in the experiment, and are separated by about 550 cm^{-1}, as sequential quanta of the bend. The inability to resolve all the peaks at higher translational energy release can be explained in two ways. First, the inherent resolution of the experiment degrades as products release more and more translational energy, which can be seen from eq 1 and is shown in Figures 10–12. Second, due to the exit impact parameter being $\sim$1 Å, the rotational widths of the vibrational peaks can become larger than 550 cm^{-1} at translational energy releases greater than 8 kcal/mol. This implies that even in a very high-resolution experiment, measuring the translational energy release may not distinguish between the different vibrational states that are produced. If, in addition to this, more than one vibrational mode in C_2H is excited by the photolysis the situation would be more complicated. This is indeed not unreasonable. A simple geometrical comparison of the ^1A_u state of C_2H_2 to the $^2\Sigma$ state of C_2H would predict bending and C–C stretching to be excited. The bend is excited because it is going from a bent to a linear state and the C–C stretch is excited because the C–C bond order increases upon going from $^1A_1$ C_2H_2 to $^2\Sigma$ C_2H. Nevertheless, it very much appears that the bending frequency of C_2H is 550 ± 100 cm^{-1} and that the nascent C_2H is produced with a large amount of energy in this degree of freedom.

C. $P(E_T)$ for $C_2H \xrightarrow{193\ nm} C_2 + H$. According to theoretical calculations there are two excited states of C_2H in the energy range of a 6.4-eV photon that are of doublet spin multiplicity.[15] These are the two lowest doublet states above the A state and are electric dipole coupled to the ground state. They are $3^2A'$ and $2^2A''$ and are both considerably bent. If one or both of these states is responsible for the secondary absorption that we are observing in C_2H, we do expect that the absorption cross section would increase for C_2H molecules that are more highly excited in the bending degree-of-freedom since the Franck–Condon factors would be higher. This is, in fact, what we have observed in the power dependence experiment.

In fluorescence emission work,[12,13] the C_2 Phillips band has been observed. This is a result of the $^1\pi_u$ state which is formed with 25 kcal/mol excess energy. In the $P(E_T)$ shown in Figure 16 it is easy to see a sharp peak at around 10 kcal/mol, which we attribute to $^1\pi_u$ of C_2. This sharp peak has underlying it a broad hump originating from one or both of two low-lying electronic states of C_2 ($^1\Sigma_g^+$ or $^3\pi_u$ or both).

D. The C–H Bond Energy in Acetylene. In previous experiments, the C–H bond energy was determined indirectly by measuring the dissociative ionization threshold for acetylene and the IP for the C_2H radical, that is processes VI and VII, re-

$$C_2H_2 \rightarrow C_2H^+ + H + e^- \quad E_{VI} \qquad \text{(VI)}$$

$$C_2H \rightarrow C_2H^+ + e^- \quad E_{VII} \qquad \text{(VII)}$$

spectively. DWM measured E_{VI} very carefully, looking at the temperature dependence of hotbands near threshold to get a value of 17.37 ± 0.01 eV. Recently, ON have disputed this value on

(19) Ho, Pauline; Bamford, Douglas J.; Buss, Richard J.; Lee, Yuan T.; Moore, C. Bradley *J. Chem. Phys.* **1982**, *76*, 3630.

(20) Jacox, Marylin E. *Chem. Phys.* **1975**, *7*, 424.

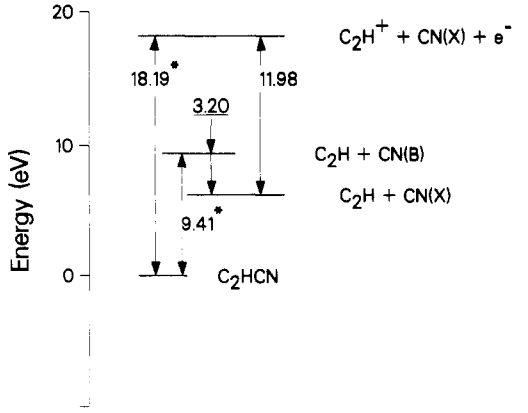

Figure 19. Energy diagram for C_2H ionization potential determination of Okabe and Dibeler (ref 6). The numbers with asterisks are the measured thresholds and the underlined numbers are well-known. The numbers with no symbols are the derived IP.

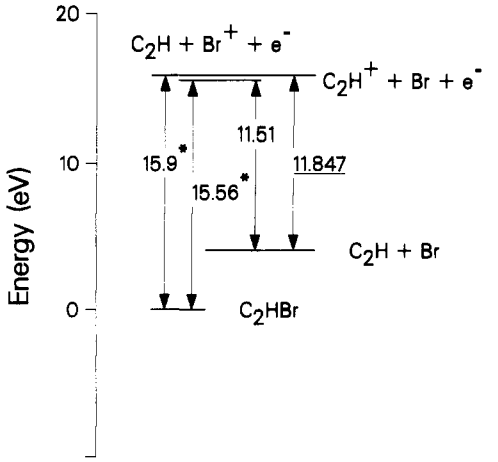

Figure 20. Same as Figure 19, but this is the work of Miller and Berkowitz (ref 7).

TABLE III

combination	C–H bond energy,[a] kcal/mol
DWM + WS	133 ± 12
DWM + MB	135 ± 1.4
DWM + OD	125 ± 1.4
ON + WS	116 ± 1.2
ON + MB	118 ± 1.8
ON + OD	107 ± 1.8

[a] This work 132 ± 2 kcal/mol.

the basis of a very sensitive molecular beam photoionization threshold measurement. ON claim the threshold to be 16.79 ± 0.03 eV.

The IP of C_2H was measured directly by Wyatt and Stafford[21] (WS) using electron-impact threshold ionization and they obtain a value of 11.6 ± 0.5 eV. In two much more precise experiments, Okabe and Dibeler[6] (OD) and Miller and Berkowitz[7] (MB) have obtained 11.96 ± 0.05 eV and 11.51 ± 0.05 eV, respectively. Their experiments are conceptually shown in Figures 19 and 20 where the numbers with asterisks are the measured values and the underlined values are well-known. Table III shows all possible values of the C–H bond energy obtained by combining in all possible ways the various experiments.

As can be seen, this work substantiates the values reported by DWM and MB. All the values calculated by using the results of ON are far too low (by about the electron affinity of H). This suggests that ON may be looking at the threshold for the ion pair production channel. It is quite possible that in the dissociative ionization of C_2HCN there is a barrier to dissociation. This would give OD a value for the IP of C_2H which is too high and consequently a $D_0(C_2H–H)$ which is too low.

As mentioned previously, our $D_0(C_2H–H)$ determination rests upon the assumption that it is possible for all available energy to appear as translation in some of the products; in other words, some of the products should be in the ground state. There are less than 20 nonrotational internal states energetically accessible in the C_2H product, even though the bending vibration is excited, and it is not likely that it would be so highly inverted that no ground state is formed. One reason for this is the light mass of the H atom. The H atom cannot impart a large impulse to the partner C_2H fragment and, hence, it cannot act to excite it vibrationally with any degree of efficiency. We believe that because of the small number of degrees of freedom and the excellent signal/noise in our data, 16.25 ± 2 kcal/mol is an accurate determination of the maximum release in translational energy and, hence, the bond energy in acetylene is found to be 132 ± 2 kcal/mol.

If Franck–Condon considerations prevent the formation of any C_2H in the vibrationless ground state, the value 132 kcal/mol would be an upper limit to the bond energy. Recently, very accurate ab initio calculations have been performed by Melius et al.[10] These have given a value of 127 kcal/mol for the bond energy. Single reference configuration calculations of this type suffer from spin contamination due to the many low-lying quartet states in this C_2H. Therefore, the error in this calculation is higher than in other molecules. In the isoelectronic case of HCN, which also has the spin contamination problem, the calculated value was slighly lower than the experimental value. This leads us to believe that 127 kcal/mol is a lower limit to $D_0(C_2H–H)$.

Janousek et al.[8] have come up with a value for $D_0(C_2H–H)$ of 132 ± 5 kcal/mol by combining processes VIII–X in a thermochemical cycle. This result is in good agreement with the present work although the uncertainty is still fairly large.

$$C_2H^- \rightarrow C_2H + e^- \quad \text{(VIII)}$$

$$C_2H_2 \rightarrow C_2H^- + H^+ \quad \text{(IX)}$$

$$H^+ + e^- \rightarrow H \quad \text{(X)}$$

Conclusions

We have measured the translatonal energy distribution for acetylene photodissociation at 193.3 nm. The primary processes are

$$C_2H_2 \xrightarrow{193\ nm} C_2H + H \quad \text{(I)}$$

$$C_2H \xrightarrow{193\ nm} C_2 + H \quad \text{(II)}$$

Process II is important even at fluences as low as 10^{26} photons/(cm^2 s). The translational energy distribution for (I) shows up to 16.25 kcal/mol translational energy release implying a $D_0(C_2H–H)$ of 132 ± 2 kcal/mol. This is the first measurement of this quantity in a single experiment. The vibrational structure of C_2H is partially resolved and we conclude that the bending frequency in C_2H is near 550 cm^{-1}. The translational energy distribution for (II) is consistent with fluorescence work showing population of $C_2(^1\pi_u, ^1\Sigma_g^+, ^3\pi_u)$.

Acknowledgment. This work was supported by the Office of Naval Research under Contract No. N00014-83-K-0069.

Registry No. C_2H_2, 74-86-2; C_2H, 2122-48-7; C_2, 12070-15-4.

(21) Wyatt, J. R.; Stafford, F. E. *J. Phys. Chem.* **1972**, *76*, 1913.